Proceedings of the 2nd International Congress APMAS2012, April 26–29, 2012, Antalya, Turkey

Characterization Investigations of W–Ni Matrix Composites Reinforced with TiB_2 and La_2O_3

H. Gökçe*, Ö. Balci, D. Ağaoğullari, Ö.U. Demirkan, A. Genç, M.L. Öveçoğlu and İ. Duman

Particulate Materials Laboratories, Department of Metallurgical and Materials Engineering
İstanbul Technical University, 34469, İstanbul, Turkey

W–1 wt% Ni (W1Ni) matrix composites reinforced with TiB_2 and La_2O_3 particles were fabricated via mechanical alloying and activated sintering methods. Powder blends with compositions of W1Ni–2 wt% TiB_2–x wt% La_2O_3 (x = 0.5, 1) were mechanically alloyed for 6 and 12 h. The results showed that increase in mechanical alloying duration to 12 h causes the decline of grain sizes of the W–Ni matrix to nanoscales. TiB_2/La_2O_3 particles have a significant effect on the density/microhardness values and wear amounts of the sintered samples.

DOI: 10.12693/APhysPolA.123.309

PACS: 81.20.Ev

1. Introduction

It is so difficult to fabricate tungsten (W) and tungsten composites due to the high melting point and low ductility of W [1]. To overcome this, activated sintering of W and W matrix composites reinforced with different carbide, nitride and oxide phases have attracted great attention in the current literature [1, 2]. Activated sintering technique enables densifications at substantially low temperatures and at short sintering durations compared with the conventional techniques [3, 4]. Reinforcing particles such as ZrC, HfC, TiC, SiC, La_2O_3, Y_2O_3, ThO_2, TiN, etc. have been used in order to improve the properties of W based composites [5–8]. However, addition of transition metal diborides as well as oxide particles is not a considerably discussed topic since only one study reported the effects of Y_2O_3 and TiB_2 particles [9]. The aim of the present study is to report the effects of TiB_2 and La_2O_3 particles on the microstructural and physical properties of W–Ni matrix.

2. Experimental procedure

Raw materials are W (Eurotungstene^{TM}, 99.9% purity, 4–7 μm), Ni (ABCR^{TM}, 99.9% purity, 3–7 μm), TiB_2 (Alfa Aesar^{TM}, 99.5% purity, 40–44 μm) and La_2O_3 (ABCR^{TM}, 99.99% purity, 25–34 μm) powders. W powders and Ni activated sintering aid (1 wt%) were mechanically alloyed (MA'd) for 6 h in order to form the pre-alloy (W1Ni) as the matrix of the composites. W1Ni matrix and 6 h pre-milled TiB_2 (2 wt%) and 6 h pre-milled La_2O_3 (0.5 and 1 wt%) powders were MA'd together for additional 6 and 12 h to constitute the W1Ni–2TiB_2–0.5La_2O_3 and W1Ni–2TiB_2–1La_2O_3 composite powders (20 g each). MA experiments were carried out in a Spex^{TM} 8000 D Mixer/Mill (1200 rpm) in a WC vial (50 ml) with WC balls (ϕ 6.5 mm) using a ball-to-powder weight ratio (BPR) of 7:1 under Ar atmosphere. All as-blended and MA'd powders were compacted in a 10 ton capacity MSE^{TM} MP-0710 uni-action hydraulic press under an uniaxial pressure of 400 MPa. These compacts were sintered at 1400 °C for 1 h in a Linn^{TM} HT-1800 furnace under Ar and H_2 gas flowing conditions.

Crystalline phases formed in the MA'd composite samples were performed by X-ray diffraction (XRD) technique using a Bruker^{TM} D8 Advanced Series Powder Diffractometer with Cu K_α radiation. The average crystallite sizes and lattice strains of the MA'd powders were determined using a TOPAS^{TM} software. Microstructures of the powders and sintered samples were observed in a Hitachi^{TM} TM-1000 SEM (15 kV) and Jeol^{TM} JEM-2000EX TEM (160 kV). Densities of the sintered samples were determined by the Archimedes method. Vickers microhardnesses were measured using a Shimadzu^{TM} HMV Microhardness Tester (100 g, 10 s). Wear experiments were conducted in a Tribotech^{TM} Oscillating Tribotester (ϕ 6 mm Al_2O_3 balls, 4 N) and abraded surfaces were characterized by a Veeco^{TM} Dektak 6 M Stylus Profiler.

3. Results and discussion

Table I shows the average crystallite sizes and lattice strains of the W powders. It reveals that all as-blended powders have nanoscale average crystallite sizes as a result of initial pre-milling step. While the La_2O_3 content has had no remarkable effect on the crystallite sizes and lattice strains, mechanical alloying durations notably affected them. It is clear to state that increase in mechanical duration results in crystalline refinement both for the W1Ni–2TiB_2–0.5La_2O_3 and W1Ni–2TiB_2–1La_2O_3 powder composites. Figure 1 represents the SEM micrograph of the W1Ni–2TiB_2–1La_2O_3 powders MA'd for 12 h revealing irregular agglomerates which are less than 1 μm.

Figure 2a and b are the bright-field (BF) and dark-field (DF) TEM micrographs (L: 100 cm) taken from the W1Ni–2TiB_2–1La_2O_3 powders MA'd for 12 h, showing spheroidal shaped particles up to about 60 nm in size. Corresponding selected-area diffraction pattern (SADP) in Fig. 2c reveals that these grains are W phase (the Bravais lattice: body centered cubic, ICDD No: 04-0806,

*corresponding author; e-mail: gokceh@itu.edu.tr

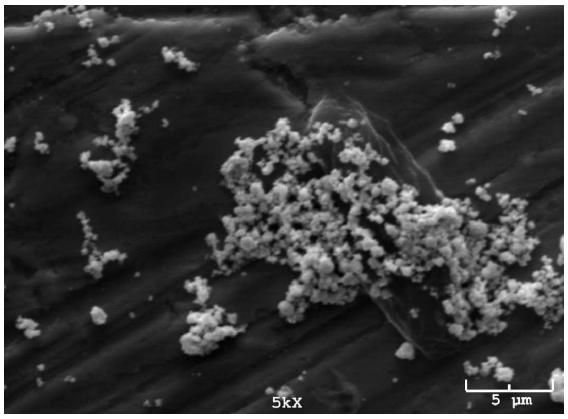

Fig. 1. SEM micrograph of the W1Ni–2TiB_2–1La_2O_3–12 h MA'd powder.

TABLE I

The average crystallite sizes and lattice strains of the W powders.

Sample name	Crystallite size [nm]	Lattice strain [%]
W1Ni–2TiB_2–0.5La_2O_3–ab	14.2	1.81
W1Ni–2TiB_2–0.5La_2O_3–6 h MA'd	8.6	2.98
W1Ni–2TiB_2–0.5La_2O_3–12 h MA'd	6.9	3.74
W1Ni–2TiB_2–1La_2O_3–ab	15.0	1.76
W1Ni–2TiB_2–1La_2O_3–6 h MA'd	10.6	2.32
W1Ni–2TiB_2–1La_2O_3–12 h MA'd	6.1	4.15

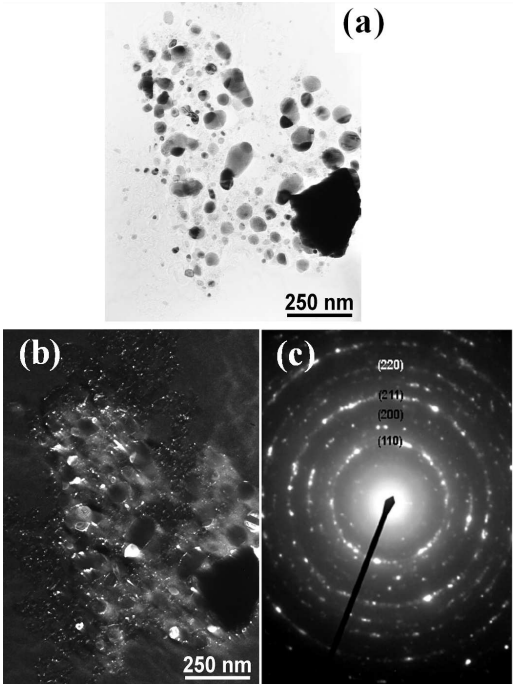

Fig. 2. TEM micrograph of the W1Ni–2TiB_2–1La_2O_3–12 h MA'd powder: (a) BF image, (b) DF image, and (c) SADP.

a = 0.316 nm). According to Fig. 2c, the microstructure consists of W grains ranging in size between 20 and 60 nm.

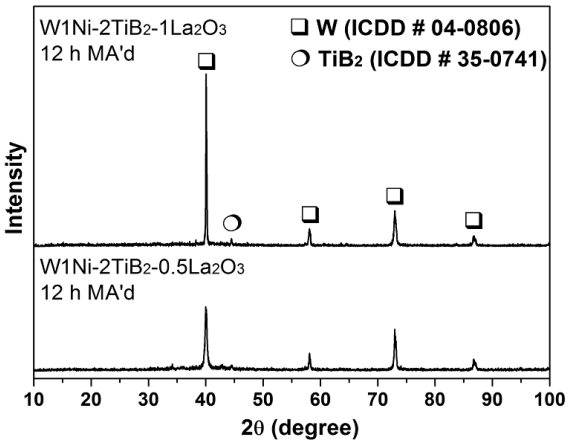

Fig. 3. XRD patterns of the sintered samples.

Figure 3 shows the XRD patterns of the sintered samples, revealing no intermetallic compound formation after sintering of the MA'd powder composites, i.e. only W and TiB_2 phases are observed. Due to their low contents in the blends, no peaks of the Ni and La_2O_3 phases exist. As seen in Fig. 4a and b, TiB_2 and La_2O_3 particles (dark contrast) are located homogeneously both at the grain boundaries and at the grain interiors in the sintered W1Ni matrix alloy (light contrast). As the La_2O_3 amount increases from 0.5% to 1% (wt), the grain size of the W1Ni matrix alloy decreases resulting from the pinning effect of La_2O_3 particles on the growth of tungsten grains.

Table II presents the relative density (RD) and the Vickers microhardness (HV) values of the sintered samples showing a significant increasing tendency both in the RD and HV values of the sintered samples with increasing MA durations. Furthermore, as the La_2O_3 amount increases from 0.5% to 1% (wt), RD and HV values of the sintered samples increase notably. It is evident from Table II that 12 h MA'd and sintered W1Ni–2TiB_2–1La_2O_3 sample has the maximum RD and HV values of 98.38% and 5.72 GPa, respectively.

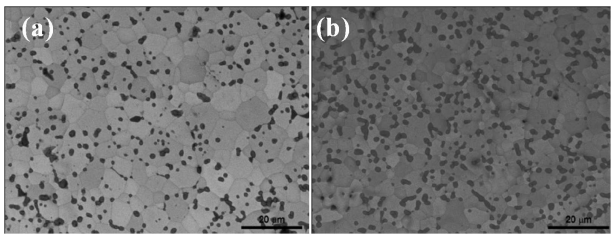

Fig. 4. BSE–SEM micrographs of the sintered samples: (a) W1Ni–2TiB_2–0.5La_2O_3–12 h MA'd, and (b) W1Ni–2TiB_2–1La_2O_3–12 h MA'd.

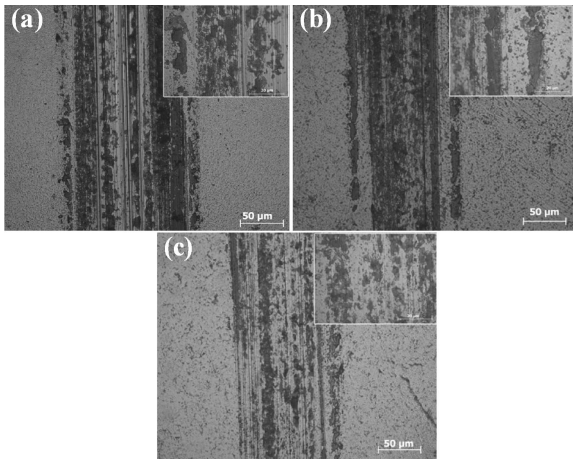

Fig. 5. Optical micrographs of the wear tracks of the sintered samples: (a) W1Ni–6 h MA'd, (b) W1Ni–$2TiB_2$–$0.5La_2O_3$–12 h MA'd, and (c) W1Ni–$2TiB_2$–$1La_2O_3$–12 h MA'd.

These values are the outcomes of small grain sizes of the W1Ni matrix shown in the TEM and SEM micrographs in Fig. 2 and Fig. 4. Moreover, HV values for each sintered composite of the as-blended and MA'd powders are higher than the sintered W1Ni matrix (4.08 GPa), indicating the positive effect of TiB_2 and La_2O_3 reinforcing particles on the properties of W1Ni matrix alloy.

Figure 5 shows the optical micrographs of the wear tracks taken from the sintered samples. The wear resistance of the sintered W1Ni sample increases significantly with the addition of TiB_2 and La_2O_3 particles. The wear rates for the sintered samples of W1Ni–6 h MA'd, W1Ni–$2TiB_2$–$0.5La_2O_3$–12 h MA'd and W1Ni–$2TiB_2$–$1La_2O_3$–12 h MA'd are 3.26 ± 0.81, 2.99 ± 0.51 and 2.11 ± 0.28 ($mm^3\ N^{-1}\ m^{-1}$) $\times 10^{-9}$, respectively. The lowest wear rate of the W1Ni–$2TiB_2$–$1La_2O_3$ sample can be explained by the nanosize W grains represented by the TEM analysis (Fig. 2).

TABLE II

Relative density (RV) and Vickers microhardness (HV) values of the sintered samples.

Sample name	Theoretical density [g/cm^3]	Relative Archimedes' density [%]	Microhardness [GPa]
W1Ni–6 h MA'd	19.08	96.39	4.08 ± 0.28
W1Ni–$2TiB_2$–$0.5La_2O_3$–ab	17.76	92.00	4.55 ± 0.30
W1Ni–$2TiB_2$–$0.5La_2O_3$–6 h MA'd		93.41	4.60 ± 0.44
W1Ni–$2TiB_2$–$0.5La_2O_3$–12 h MA'd		95.90	5.09 ± 0.28
W1Ni–$2TiB_2$–$1La_2O_3$–ab	17.60	89.96	4.48 ± 0.11
W1Ni–$2TiB_2$–$1La_2O_3$–6 h MA'd		98.10	5.34 ± 0.18
W1Ni–$2TiB_2$–$1La_2O_3$–12 h MA'd		98.38	5.72 ± 0.19

4. Conclusions

In this study, the effects of TiB_2 and La_2O_3 content and mechanical alloying duration on the microstructural and physical properties of the activated sintered W–1 wt% Ni matrix alloy were investigated. The average crystallite sizes of the powder blends and W grains decrease to nanosizes with increasing MA durations. The addition of TiB_2 and La_2O_3 particles and the decline in grain size of W matrix have a positive effect on the density/microhardness values and wear amounts of the samples. The best results for relative density, microhardness value and wear resistance were obtained from the 12 h MA'd and sintered W1Ni–$2TiB_2$–$1La_2O_3$ sample.

Acknowledgments

The authors would like to acknowledge the Scientific and Technological Research Council of Turkey (TUBITAK) for funding the project with the number 110M130.

References

[1] E. Lassner, W.D. Schubert, *Tungsten: Properties, Chemistry, Technology of the Element, Alloys and Chemical Compounds*, Kluwer Academic, New York 1999.

[2] H.W. Hayden, J.H. Brophy, *J. Electrochem. Soc.* **110**, 805 (1963).

[3] N.M. Hwang, Y.J. Park, D.Y. Kim, D.Y. Yoo, *Scr. Mater.* **42**, 421 (2000).

[4] S.W. Kim, S.I. Lee, Y.D. Kim, I.H. Moon, *Int. J. Refract. Met. H* **21**, 183 (2003).

[5] G.M. Song, Y.J. Wang, Y. Zhou, *Mater. Sci. Eng. A* **334**, 223 (2002).

[6] Y. Chen, Y.C. Wu, F.W. Yu, J.L. Chen, *Int. J. Refract. Met. H* **26**, 525 (2008).

[7] K.E. Rea, V. Viswanathan, A. Kruize, J.Th.M. de Hosson, S. O'Dell, T. McKechnie, S. Rajagopalan, R. Vaidyanathan, S. Seal, *Mater. Sci. Eng. A* **477**, 350 (2008).

[8] S. Coşkun, M.L. Öveçoğlu, B. Özkal, *J. Alloys Comp.* **492**, 576 (2010).

[9] A. Genç, S. Coşkun, M.L. Öveçoğlu, *Mater. Char.* **61**, 740 (2010).